Complex-valued intermolecular coupling enables directional exciton transport in excitonic circuits

Maria A. Castellanos and Adam P. Willard*

Department of Chemistry, Massachusetts Institute of Technology, Cambridge, MA 02139, USA

E-mail: awillard@mit.edu

Abstract

Molecular systems capable of directing the flow of excitons are key to the development and optimization of optoelectronic materials. The transport of excitons across multiple molecules is governed by the intermolecular electronic coupling network. In this manuscript, we consider the effects of complex-valued intermolecular electronic coupling on exciton transport. We present a molecular motif capable of generating complex-valued coupling under excitation with circularly polarized light. We use theoretical modeling and simulation to illustrate how complex coupling can be leveraged to drive the rotational flux of excitons in cyclic molecular networks and direct exciton population at branched molecular networks.

1 Introduction

A system of semiconducting moieties, such as organic dye molecules, conjugated oligomers, or quantum dots, can be arranged to form a circuit capable of conducting the flow of excited

electron-hole pairs, otherwise known as excitons. The tendency of excitons to migrate or delocalize within such a circuit is mediated by the intermolecular electronic coupling network. In principle, unique modes of control over exciton dynamics can be achieved when elements of this network are complex-valued. This includes the ability to direct the flow of excitons to turn in specific directions within cyclic or branching circuits. Currently, however, little is known about how to generate complex-valued coupling (CVC) in realistic multichromophoric excitonic systems. In fact, standard models of intermolecular electronic coupling, such as Förster theory, appear to exclude the possibility of realizing CVCs.[1,2]

In this manuscript, we present a strategy for designing excitonic circuits that exhibit complex-valued coupling elements. We demonstrate the physical viability of such circuits by proposing a simple molecular motif capable of yielding CVCs, and we suggest a strategy for producing and observing their effects in a laboratory setting. We then highlight the unique capabilities of circuits with CVCs to direct the flow of excitons using a simplified site-based model.

Control over exciton dynamics is important for enabling the transport and conversion of optical excitation energy in semiconducting systems. Excitonic circuits are molecular systems that provide this control. Natural photosynthetic systems have evolved to include excitonic circuits that efficiently shuttle the energy of absorbed sunlight from light-harvesting complexes to the reaction center (where the water-splitting reaction is catalyzed).[3,4] In artificial system, excitonic circuits can be designed to improve the performance of the broad array of technologies that utilize the properties of excitons. This includes applications in photovoltaics,[5,6] photocatalysis,[7] imaging,[8,9] signal processing,,[10] solid state lighting,[11,12] and quantum information processing.[13,14]

In this study, we limit our focus to excitonic circuits made up of multiple organic dye molecules, which we herein refer to as chromophores. In close contact, certain species of chromophores can couple strongly enough to permit exciton delocalization and diffusion across $\sim$10s or $\sim$100s of molecules within typical exciton lifetimes.[15,16] While the general tendency

for exciton diffusion can be tuned via the intermolecular coupling strength, the directionality of diffusion is less easily controlled.[14] The most reliable strategy for generating direction exciton transport is to design circuits with internal energy gradients. This strategy is effective, but necessitates performance loss in applications that require high energy conversion efficiency.[17] By utilizing CVCs, excitonic circuits can be designed to promote directional transport without necessitating dissipative energy loss.

Our approach to generating CVCs relies on control over the phase of the excitonic wavefunction. When the state of an exciton has a distinct phase, its coupling to other excitonic states can depend on this phase. Through this dependence, the coupling elements between excitonic states can be complex-valued. The challenges we address in this work are thus to determine (1) how to design systems of chromophores that support excitons with controllable phase, and (2) how to formulate the intermolecular coupling so that it includes the effects of this phase.

This manuscript is organized as follows. We begin, in the next section, with a brief review of the topic of phase in quantum systems. Then, in Sec. 3 we introduce a system of two chromophores capable of generating CVCs. We formalize this system using the Frenkel-Dovydov model and simulate the emergence of CVC via optical excitation with circularly polarized light. In Sec. 4, we present several model systems capable of manipulating the directional flow of excitons with CVCs. Finally, prior to concluding, we discuss some effects of non-ideality on the performance of these systems.

2 Phase in quantum systems.

The ability of quantum mechanical objects, such as electrons or excitons, to interfere is determined by the relative phase of their wavefunctions. In the simple case of a quantum two-level system, this phase can be defined by a single angle, ϕ, which specifies the longitudinal orientation of the wavefunction as represented on the Bloch sphere. This phase angle

constitutes the complex character of the wavefunction,

$$|\psi\rangle = \cos\left(\frac{\theta}{2}\right)|0\rangle + e^{i\phi}\sin\left(\frac{\theta}{2}\right)|1\rangle, \tag{1}$$

where $|0\rangle$ and $|1\rangle$ are the two states (*e.g.*, spin-up and spin-down) and θ defines the latitudinal orientation of the vector representing the wavefunction on the Bloch sphere.

Similarly, the complex-valued components of electronic wavefunctions are associated with phase angles, and likewise are responsible for electronic interference, such as exhibited in electron diffraction patterns.[18] The phase of an electronic wavefunction can be externally manipulated via electromagnetic potentials. For instance, the Aharonov–Bohm (AB) effect describes how an electron experiences a phase shift when circulating in the presence of a magnetic field.[19] This particular effect has been utilized to enable quantum computing operations and information storage on multi-spin systems[20,21] and semiconductor quantum rings,[22,23] and to increase the efficiency of electron transport in light-harvesting models.[24–26]

An exciton comprises an electron and a hole. The electron and hole wavefunctions both contain spatially varying phases, reflecting the nodal symmetries of the frontier molecular orbitals, the LUMO and HOMO, respectively. This phase variation is evident in the renderings of HOMO and LUMO orbitals that are often produced from molecular electronic structure calculations. This spatially varying phase is responsible for certain excitonic phenomena, such as the strong sensitivity of charge-transfer coupling to intermolecular twist angle in π-stacked homo-dimers.[27,28]

An exciton can also acquire phase during delocalization, whereby the wavefunction oscillates between different exciton basis states. This phase can be formulated within a complex superposition of basis states and is notably distinct from that which characterizes molecular orbital structure. Our approach to generating CVCs utilizes this kind of complex superposition phase. In particular, we leverage a superposition state that arises when certain highly symmetric chromophores are excited with circularly polarized light. As we describe in the

following section, the phase associated with this superposition can dress the intermolecular electronic coupling to external chromophores, and thereby yield CVCs.

3 A dimer system for generating complex-valued couplings

In this section, we present a two-chromophore system capable of generating CVCs under excitation with circularly polarized light. We formalize the excitonic properties of this system using the Frenkel-Davydov (FD) model. In this model, the exciton is described in a reduced basis of interacting states via the excitionic Hamiltonian,

$$H_{\text{ex}} = \sum_{n=1}^{N} E_n |n\rangle + \sum_{n \neq m}^{N} V_{nm} |n\rangle\langle m|, \tag{2}$$

where $|n\rangle$ denotes the nth basis state, E_n is the energy of the exciton in that state, and V_{nm} is the coupling between states $|n\rangle$ and $|m\rangle$.[29,30] Despite its formal simplicity, the FD model has been repeatedly shown to accurately reproduce experiments across a wide range of chemical systems.[16,31,32]

In typical applications of the FD model, each basis state is chosen to represent the lowest energy singlet excitation of a given chromophore, with all other chromophores assumed to be in their electronic ground state. With this choice of basis, the parameters E_n and V_{nm} are easily interpretable as the excitation energy of chromophore n and the electronic coupling between chromophores n and m, respectively. These parameters depend on the atomistic details of the system and can be derived from theory or computed via first-principles calculation.[14,33]

Our two-chromophore system for generating CVCs comprises one standard chromophore, such as a Cy3 dye molecule, contributing a single exciton basis state, and one high-symmetry chromophore, such as a metal-porphyrin, contributing a degenerate pair of exciton basis

states. For the standard chromophore, the exciton state represents a typical HOMO-to-LUMO ($\pi \rightarrow \pi^*$) electronic transition. We will refer to this type of chromophore as a *linear chromophore* because the transition dipole vector (TDV) tends to align with the long axis of the conjugated system of atoms. For the high-symmetry chromophore, we consider a molecule with a π-electron system that is both cyclic and symmetric, specifically, possessing $\mathrm{D_{Nh}}$ symmetry. We will refer to this type of chromophore as a *circular chromophore* due to the cyclic nature of the conjugated system of atoms. In an idealized nuclear configuration, the LUMO level of a circular chromophore contains a pair of degenerate π^* orbitals. The TDVs associated with these two $\pi \rightarrow \pi^*$ electronic excitations are orthogonal and oriented within the plane of the π system. We hereby allow these vectors to define the orientation of the x and y axes.

We label the single state of the linear chromophore as $|\mathrm{L}\rangle$ and the two states defined by the TDV of the circular chromophore as $|x\rangle$ and $|y\rangle$. The excitonic Hamiltonian of the dimer comprising one *linear* and one *circular* chromophore, in matrix form, is thus given by,

$$H_{\mathrm{ex}}^{(xy)} = \begin{pmatrix} E_{\mathrm{L}} & V_{\mathrm{L}x} & V_{\mathrm{L}y} \\ V_{x\mathrm{L}} & E_{\mathrm{C}} & 0 \\ V_{y\mathrm{L}} & 0 & E_{\mathrm{C}} \end{pmatrix}, \tag{3}$$

where $E_{\mathrm{C}} = E_x = E_y$ and the coupling between states $|x\rangle$ and $|y\rangle$ is zero by orthogonality. The values of $V_{\mathrm{L}x}$ and $V_{\mathrm{L}y}$ in this matrix represent the Coulomb interaction between the transition densities of state $|\mathrm{L}\rangle$ and state $|x\rangle$ or $|y\rangle$ and would therefore be real-valued. Within the point-dipole approximation, the coupling can be expressed in terms of the relative orientations of the linear and cyclic chromophores. For instance,

$$V_{\mathrm{Lx}} = V_x \left[\hat{\mu}_{\mathrm{L}} \cdot \hat{\mu}_{\mathrm{x}} - 3(\hat{\mu}_{\mathrm{L}} \cdot \hat{r})(\hat{\mu}_{\mathrm{x}} \cdot \hat{r})\right], \tag{4}$$

where $\hat{\mu}_{\mathrm{L}}$ and $\hat{\mu}_{\mathrm{x}}$ are the unit vectors indicating the orientations of the TDVs of $|\mathrm{L}\rangle$ and

$|x\rangle$, $\hat{r}$ is the unit vector of the center-to-center separation between the linear and circular chromophores, and V_x parameterizes the effective coupling strength, which depends on both the separation and relative orientations of the TDVs. An analogous expression describes V_{Ly}. To further simplify the formalism, we will assume that $\hat{r} = \hat{z}$ (*i.e.*, that the dimer pair is separated along the z-axis, and that $\hat{\mu}_{\mathrm{L}} \cdot \hat{z} = 0$). With these assumptions, the couplings each reduce to a simple function of single angular coordinate,

$$V_{\mathrm{Lx}} = V_x \cos(\theta), \tag{5}$$

and

$$V_{\mathrm{Ly}} = V_y \sin(\theta), \tag{6}$$

where θ is the angle between $\hat{\mu}_{\mathrm{L}}$ and the x-axis, as illustrated in Fig. 1B.

Notably, the dipole approximation invoked above, nor the assumption that the two chromophores are aligned along the z axis, is necessary to model this dimer system. Indeed, the value of V_{Lx} and V_{Ly} could be determined more accurately from first-principles calculation. However, the above approximations allow us to generate simple expressions to guide intuition and enables a straightforward (albeit approximate) examination of how changes in the geometric arrangement of the dimer pair modify the effects of CVCs.

In this system, CVCs emerge under excitation with circularly polarized light. Under this excitation condition, the basis states $|x\rangle$ and $|y\rangle$ are not independently excitable. Rather, circularly polarized photons excite complex superpositions of the $|x\rangle$ and $|y\rangle$ states. This has been demonstrated for Mg-porphyrin (possessing $D_{4\mathrm{h}}$ symmetry).[34–36] The appropriate basis states for describing these superpositions are the eigenstates of the angular momentum operator, $|+\rangle$ and $|-\rangle$, defined as,

$$|\pm\rangle = \frac{1}{\sqrt{2}} \left(|x\rangle \pm i|y\rangle \right). \tag{7}$$

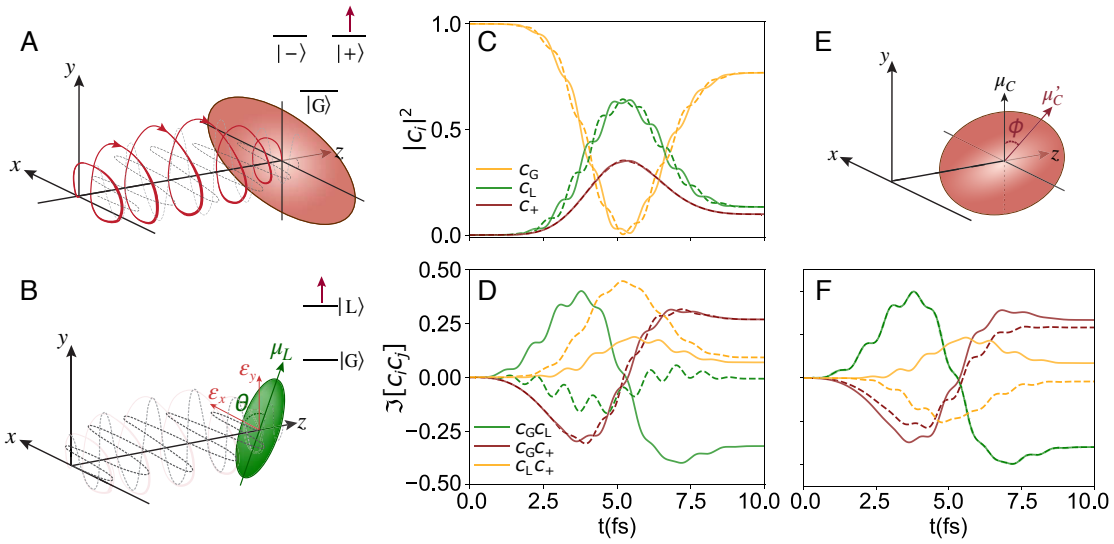

Figure 1: (A) A circularly polarized pulse propagating in the z axis acts on a molecule with D_{Nh} symmetry (*circular* molecule), populating one of two delocalized excitations. Here the pulse is depicted as RCP and creates an exciton localized in the $|+\rangle$ state. (B) Schematic representation of the pulse acting on a molecule, which populates the first excited state. Unlike the *circular* molecule, the x and y components of the linear molecule's dipole moment, μ_{L}, are not symmetric and will interact with the corresponding components of the circular pulse (ε_x and ε_y, respectively) separately, according to the dipole angle with respect to the x axis, θ. (C) Time evolution of populations and (D) coherences of an exciton shared between a porphyrin and Cy3 molecules, after a RCP circularly polarized pulse is applied, as described in the text. Solid lines correspond to a choice of $\theta = 0$ and dashed lines to $\theta = \pi/2$. (E) A D_{Nh} symmetric molecule when the molecular (xy) plane is not orthogonal to the axis of propagation. The deviation is quantified by the angle ϕ. (F) Time evolution of the coherences for the dimer wavefunction when $\theta = 0$ and $\phi = 0$ and $\pi/3$ (solid and dashed lines, respectively).

To model excitons generated from circularly polarized light, we thus perform a change of basis from the states ($|\mathrm{L}\rangle$, $|x\rangle$, $|y\rangle$) to ($|\mathrm{L}\rangle$, $|+\rangle$, $|-\rangle$). The resulting FD Hamiltonian is,

$$H_{\mathrm{ex}}^{(\pm)} = \begin{pmatrix} E_{\mathrm{L}} & V_{\mathrm{L}+} & V_{\mathrm{L}-} \\ V_{+\mathrm{L}} & E_{\mathrm{C}} & 0 \\ V_{-\mathrm{L}} & 0 & E_{\mathrm{C}} \end{pmatrix}, \tag{8}$$

where the elements $V_{\mathrm{L}+}$ and $V_{\mathrm{L}-}$ represent the coupling between $|\mathrm{L}\rangle$ and $|+\rangle$ and $|-\rangle$, respectively. The values of these coupling elements can be expressed as $V_{\mathrm{L}+} = \frac{1}{\sqrt{2}}\left(V_{\mathrm{L}x} + iV_{\mathrm{L}y}\right)$ and $V_{\mathrm{L}-} = \frac{1}{\sqrt{2}}\left(V_{\mathrm{L}x} - iV_{\mathrm{L}y}\right)$. Substituting Eqs. 5 and 6 yields expressions that contain a phase angle,

$$V_{\mathrm{L}+} = \frac{1}{\sqrt{2}}\left(V_x \cos(\theta) + iV_y \sin(\theta)\right), \tag{9}$$

and,

$$V_{\mathrm{L}-} = \frac{1}{\sqrt{2}} \left(V_x \cos(\theta) - i V_y \sin(\theta) \right), \tag{10}$$

with $V_{+\mathrm{L}}$ and $V_{-\mathrm{L}}$ equal to the complex conjugates of $V_{\mathrm{L}+}$ and $V_{\mathrm{L}-}$, respectively.

Note that the phase will only appear in the interaction when the circularly-polarized molecule is coupled to a low-symmetry molecule. For a pair of circularly-polarized high-symmetry molecules, the frame of reference for the dipole moments is indistinguishable, which leads to phase cancellation, while two linear molecules excited through circularly polarized light do not yield a complex-valued superposition excited state.

3.1 Simulating the optical excitation of the CVC dimer system.

The expressions in Eqs. 9 and 10 reveal that CVCs can emerge when exciton states are initialized with circularly polarized light. In this section, we carry out a simulation to verify that the $|+\rangle$ and $|-\rangle$ states can be selectively populated when the circular-linear dimer system is subject to a pulse of circularly polarized light.

To model photoexcitation, we utilize a FD model that is extended to include the electronic ground state. We denote the ground state as $|G\rangle$ and the three exciton basis states as we have previously, *i.e.*, $|\mathrm{L}\rangle$, $|+\rangle$, and $|-\rangle$. Following the model described in Ref. 34, we write the wavefunction for the 4-state exciton system as,

$$\begin{aligned} |\Psi(t)\rangle =& c_{\mathrm{G}}(t)|\mathrm{G}\rangle \\ &+ c_{\mathrm{L}}(t)|\mathrm{L}\rangle e^{-iE_{\mathrm{L}}t/\hbar} \\ &+ c_{+}(t)|+\rangle e^{-iE_{\mathrm{C}}t/\hbar} \\ &+ c_{-}(t)|-\rangle e^{-iE_{\mathrm{C}}t/\hbar}. \end{aligned} \tag{11}$$

We study the evolution of $|\psi(t)\rangle$ when the system is perturbed by a circularly polarized laser field $\varepsilon_{\pm}(t)$. We simulate the evolution via the time-dependent Schrödinger equation under

the dipole approximation,

$$i\hbar|\dot{\Psi}(t)\rangle = \left(H_{\text{ex}}^{(\pm)} - \hat{\mu}\cdot\varepsilon_{\pm}(t)\right)|\Psi(t)\rangle, \tag{12}$$

where $\hat{\mu}$ is the dipole moment operator. The right/left circularly polarized pulse (RCP/LCP) is described in terms of its Cartesian components,

$$\varepsilon_{\pm}(t) = \varepsilon_0 s(t)[\cos(\omega t+\eta)\hat{e}_x \pm \sin(\omega t+\eta)\hat{e}_y], \tag{13}$$

with field amplitude ε_0, carrier frequency ω, phase η, unit vectors $\hat{e}_x$ and $\hat{e}_y$ along the x- and y-axes and shape function $s(t) = \sin^2\left(\frac{\pi t}{t_p}\right)$, with t_p the duration of the pulse.

We assume the circularly polarized light pulse propagates along the z-axis and that the circular chromophore is oriented perpendicular to the pulse (*i.e.*, aligned with the xy-plane). The linear chromophore is positioned with its TDV oriented in the xy-plane and rotated by an angle θ relative to the x axis. We then derive expressions for the coefficients $c_i(t)$ in the presence of a RCP with frequency resonant to the excitation energy of the circular chromophore, $\omega_{\text{C}} = E_{\text{C}}/\hbar$. The derivation, presented in full detail in the SI, results in the following expression,

$$\dot{c}_{\text{G}}(t) = \frac{i}{\hbar}\varepsilon_0 s(t)\left(|\mu_{\text{L}}|\cos(\theta-\omega_{\text{C}}t)c_{\text{L}}(t)e^{-i\omega_{\text{L}}t} + \mu_{\text{C}}c_{+}(t)\right), \tag{14a}$$

$$\dot{c}_{\text{L}}(t) = \frac{i}{\hbar}\varepsilon_0 s(t)\left(|\mu_{\text{L}}|\cos(\theta-\omega_{\text{C}}t)c_{\text{G}}(t)e^{i\omega_{\text{L}}t}\right), \tag{14b}$$

$$\dot{c}_{+}(t) = \frac{i}{\hbar}\varepsilon_0 s(t)\mu_{\text{C}}c_{\text{G}}(t), \tag{14c}$$

$$\dot{c}_{-}(t) = 0, \tag{14d}$$

where $\omega_{\text{L}} = E_{\text{L}}/\hbar$. From this system of ODEs, we note that the dipole angle, θ, adds a phase to the circularly polarized field acting on the linear exciton, with the coefficient evolving as $c_{\text{L}}(t)$. When the same pulse interacts with the *linear* chromophore, the equal-magnitude x and y components of the field interact with the components of the dipole vector separately,

weighted by the relative angle of the dipole, θ, as described by Equations 5 and 6.

The ODE system in Eq. 14 does not have a straightforward analytical solution, therefore we provide a numerical solution for the system of equations using the molecular and pulse parameters from Ref. 34: $\varepsilon_0 = 2.20 \times 10^9$ Vm^{-1} and $s(t) = \sin^2\left(\frac{\pi t}{t_p}\right)$, with $t_p = 9.67$ fs the duration of the pulse. The *circular* molecule is chosen to be Mg-Porphyrin, with $\mu_{\mathrm{C}} = -1.84$ ea_0 and $\hbar\omega = 2.21$ eV, and the *linear* molecule to be Cy3 ($\mu_{\mathrm{L}} = 5.04$ ea_0 and $\hbar\omega = 2.27$ eV). The resulting populations, $|c_i|^2$, and coherences as given by the imaginary components of $c_i c_j$, *i.e.*, $\mathcal{I}[c_i c_j]$, between the four states are shown in Fig. 1C and D, for $\theta = 0$ (solid) and $\theta = \pi/2$ (dashed). As our model indicates, the phase will almost exclusively affect the formation of the linear exciton state, $|\mathrm{L}\rangle$. This effect is especially apparent in the exciton coherences (Fig. 1D). Note that in our model the *linear* exciton state populates more than the *circular* due to the linear chromophore having a larger transition dipole.

In the model presented above, we assumed an idealized geometry in which the axis of light propagation is perpendicular to the plane of the *circular* chromophore. To explore the effects of the relative alignments of the light pulse and the circular chromophore, we consider an expanded model in which the linear chromophore is tilted out of the xy-plane by an angle ϕ, as depicted in Fig. 2. With this model, derived in full detail in the SI, the evolution of the excitonic wavefunction is given by the following system of equations.

$$\dot{c}_{\mathrm{G}}(t) = \frac{i}{\hbar}\varepsilon_0 s(t)\left(|\mu_{\mathrm{L}}|\cos(\theta - \omega_{\mathrm{C}}t)c_{\mathrm{L}}(t)e^{-i\omega_{\mathrm{L}}t} + \mu_{\mathrm{C}}e^{i\phi}c_{+}(t)\right) \tag{15a}$$

$$\dot{c}_{\mathrm{L}}(t) = \frac{i}{\hbar}\varepsilon_0 s(t)\left(|\mu_{\mathrm{L}}|\cos(\theta - \omega_{\mathrm{C}}t)c_{\mathrm{G}}(t)e^{i\omega_{\mathrm{L}}t}\right) \tag{15b}$$

$$\dot{c}_{+}(t) = \frac{i}{\hbar}\varepsilon_0 s(t)\mu_{\mathrm{C}}e^{-i\phi}c_{\mathrm{G}}(t) \tag{15c}$$

$$\dot{c}_{-}(t) = 0 \tag{15d}$$

In these equations, we find that the effect of the alignment angle ϕ is to impose a global phase on the evolution of the $|+\rangle$ basis state. Excitation with a LCP pulse imposes an analogous phase shift on the $|-\rangle$ basis state. Numerical solutions to these equations for

$\theta = 0$ and $\theta = \pi/3$ are presented in Fig. 1F as dashed lines. The coherences, $\mathcal{I}[c_i c_j]$ for $\phi = \pi/3$ compare to those for a perfectly aligned system with $\phi = 0$ and $\theta = 0$. Populations $|c_i|^2$ for an arbitrary alignment given by ϕ will be identical to those of the $\phi = 0$ dimer. These findings show that in a linear-circular excitonic circuit, the population dynamics only depend on the relative geometry of the linear chromophore, as defined by angle θ. The relative orientation of the circular chromophore does not affect population dynamics.

4 Exciton dynamics in CVC-containing model systems

4.1 Two-chromophore model system

To evaluate the influence of CVCs on excitonic circuits, we first consider the dynamics of an exciton on a dimer pair with CVC. To simplify the modeling and interpretation, we consider a FC model with only two excitonic basis states, effectively isolating $|+\rangle$ or $|-\rangle$ into a single active state. The corresponding Hamiltonian matrix is given by,

$$\hat{H}_{\text{dimer}} = \begin{pmatrix} E_{\text{L}} & V_{\text{LC}} \\ V_{\text{CL}} & E_{\text{C}} \end{pmatrix} \tag{16}$$

where $V_{\text{LC}} = V_{\text{L}+}$, when a RCP pulse is applied, and $V_{\text{L}-}$, when a LCP pulse is used, as defined in Eq. 9 and 10, respectively. We also note, $V_{\text{CL}} = V_{\text{LC}}^*$. As before, we choose $E_{\text{C}} = \hbar\omega_{\text{C}}$ to be the excitation energy of Mg-Porphyrin and $E_{\text{L}} = \hbar\omega_{\text{L}}$ that of a Cy3 dye. Arbitrary values for the real components of the coupling are set to be proportional to the energy difference between the two Frenkel exciton states, $V_x = \Delta E_{\text{LC}}/2$ and $V_y = 3\Delta E_{\text{LC}}/4$, with $\Delta E_{\text{LC}} = E_{\text{L}} - E_{\text{C}}$. The dimer system is illustrated in Fig. 2A. Note that we set V_x and V_y to different values, as the system described by $V_x = V_y = |V|$ evolves independently to the angle θ (Figure S1).

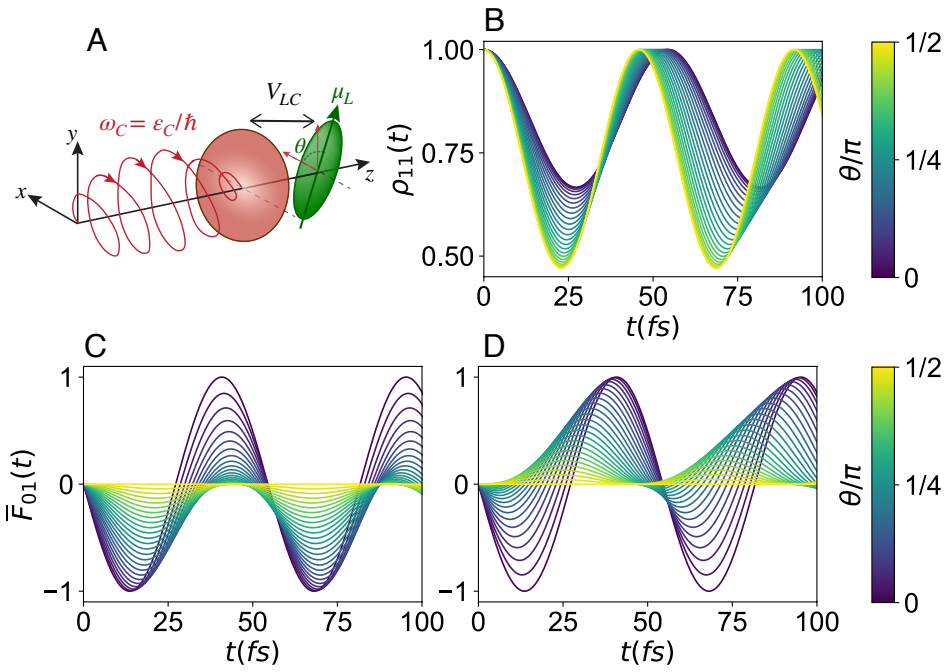

Figure 2: (A) Representation of a dimer with imaginary excitonic coupling. A coupled pair comprising an aromatic ring with D_{Nh} symmetry and a molecule with a linear transition dipole vector μ_L is excited via a circularly polarized pulse resonant with the first excitation of the first molecule, $\omega_C = E_C/\hbar$. (B) Exciton populations for the dimer as the phase angle θ is varied. The normalized excitonic flux, $\overline{F}_{01}$, is shown for a (C) RCP and (D) LCP incident pulse.

We simulate the evolution of an exciton via the Liouville equation,

$$\dot{\rho} = -\frac{i}{\hbar}\left[\hat{H}, \rho(t)\right] \tag{17}$$

where ρ is the density matrix describing the state of the closed system. To model the dimer system, we use $\hat{H}_{\text{dimer}}$ as the Hamiltonian in Eq. 16. The expression above leads to a system of ODEs for the matrix elements of the density matrix, which can be solved to obtain the population dynamics of the exciton (i.e., the diagonal elements of the density matrix ρ). The resulting system of equations can be found in the Supporting Information. We initialize the system with the exciton fully localized on the circular chromophore (*i.e.*, $\rho_{11} = 1$ and $\rho_{22} = 0$). Figure 2B contains a plot of the population on the circular chromophore over time for a range of different inter-chromophore angles, θ.

The populations $\rho_{ii}(t)$ provide information about the occupation of the exciton at a given

time but do not report on the process of coherent exciton transfer between the chromophores. For instance, if we treat the coupling as a global phase $V_{\mathrm{LC}} = |V_0|e^{i\theta}$ (*i.e.*, corresponding to the case where $V_x = V_y = V_0$), the populations are predicted to be independent of the phase angle. As expanded upon in the Supporting Information, when the initial state of the system is localized on one of the molecules, the factor will merely act as an overall phase in the evolution of the site-basis probability amplitudes, $c_i(t)$. On the other hand, the imaginary part of the off-diagonal elements of the density matrix, $\mathcal{I}[\rho_{ij}]$, contains information about the quantum coherence and therefore the direction of the exciton flux. As seen in Fig. S1, the coherences for the $V_x = V_y$ case do depend on the phase θ.

To define the directionality of flow in exciton population, we compute the quantity,

$$F_{mn} = 2V_{mn}\mathcal{I}[\rho_{mn}], \tag{18}$$

which quantifies the exciton flux between molecules m and n.[37] In this expression, the sign of F_{mn} specifies the direction of the coherent exciton transfer, with $F_{mn} > 0$ indicating transfer from m to n. The exciton flux is normalized by scaling each value to its maximum magnitude, $\overline{F}_{mn}$, and calculated for the dimer as a function of θ for both RCP and LCP light as plotted in Fig. 2B and C, respectively. We observe, except in the limiting cases of $\theta = 0$ and $\theta = \pi$, that $F_{mn}^{(\mathrm{RCP})}(t) \neq -F_{mn}^{(\mathrm{LCP})}(t)$, indicating that inverting the polarization of the pulse will not simply shift the direction of the exciton flux, but will also affect the magnitude of flux at a given time.

Environmental noise tends to have a detrimental effect on processes that rely on exciton coherence. To assess the role that noise may play in our system, we applied Redfield theory to simulate the behavior of the dimer system when it is weakly coupled to a bath.[38] Following the equations outlined in Sec. S4.1, we choose parameters for the Redfield equation within a range observed typically for organic chromophores systems at 300K. For the bath spectral density (Eq. S17) we set $\lambda = 100$ cm^{-1} and Ω_c to be proportional to λ by $2\lambda/(\beta\Omega_c^2) = 1.2$.[14]

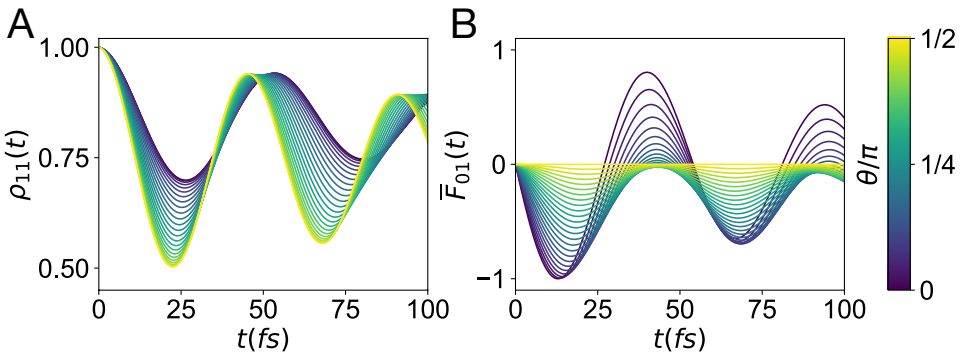

Figure 3: (A) Exciton population for the dimer depicted in Fig. 2 when the system is in contact with a harmonic bath, at different angles of alignment θ. (B) Normalized flux $\bar{F}_{01}$ for the same system. Here all chromophores are coupled to a bath with dephasing rate γ=0.1

Figure 3 shows the populations for the dimer when each chromophore interacts with a separate harmonic bath with a dephasing rate $\gamma = 0.1$. As expected, the oscillations in the dimer populations and excitonic fluxes are damped out by the bath within the first ~ 100 fs.

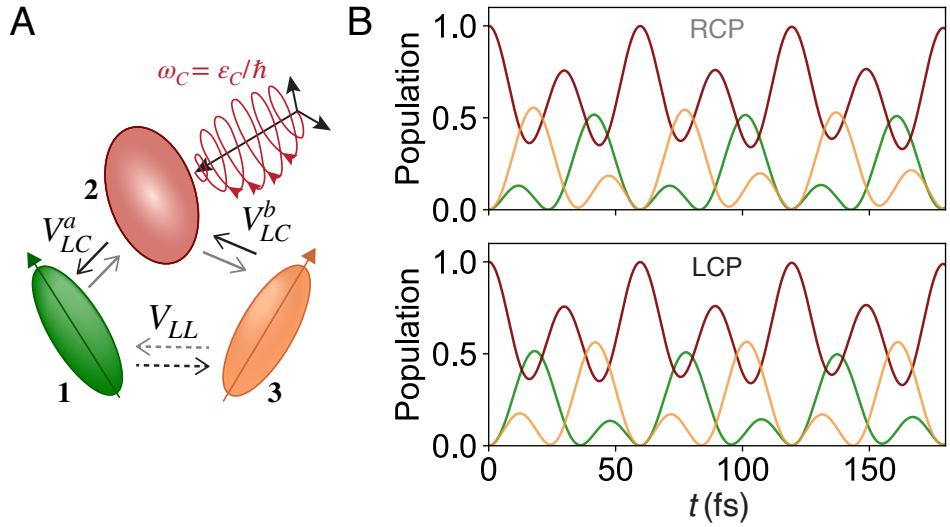

Figure 4: (A) The three-chromophore cycle system described in Eq. 19. One chromophore with $D_{N\mathrm{h}}$ symmetry is excited with circularly polarized light (red circle) and is coupled with two of low-symmetry (a and b). (B) For two linear chromophores with different relative orientations with respect to the circular molecule, $\theta_a \neq \theta_b$, inverting the direction of the light will change the order at which an exciton initially localized at **1** populates the other two sites.

4.2 Three-chromophore cyclic circuit.

We now consider the dynamics of an exciton in a cyclic circuit comprised of three chromophores - one circular chromophore and two linear chromophores. The geometry of the system is illustrated in Fig. 4A. This system is defined by the following Frenkel Hamiltonian,

$$\hat{H}_{\text{trimer}} = \begin{pmatrix} E_{\text{L}}^{a} & V_{\text{LC}}^{a} & V_{\text{LL}} \\ V_{\text{CL}}^{a} & E_{\text{C}} & V_{\text{LC}}^{b} \\ V_{\text{LL}} & V_{\text{CL}}^{b} & E_{\text{L}}^{b} \end{pmatrix}. \tag{19}$$

where E_{C} is the excitation energy of the circular chromophore, and E_{L}^{a} and E_{L}^{b} are the excitation energies of the two linear chromophores (labeled a and b). In this system, the linear-circular coupling, V_{LC}, carries a complex phase *e.g.*, as in Eq. 9, while the linear-linear interaction V_{LL} does not. Specifically, $V_{\text{LC}}^{a} = \cos\theta_a V_x \pm \sin\theta_a V_y$, with a similar expression for V_{LC}^{b}.

We simulated the evolution of an exciton in a closed three-chromophore cyclic circuit via the Liouville equation (Eq. 17), with the exciton initially localized on the cyclic chromophore. The results of this simulation are plotted in Fig. 4 for excitation via right-hand or left-hand circularly polarized light, when the *linear* molecules a and b are oriented relative to the *circular* molecule according to $\theta_a = 3\pi/4$ and $\theta_b = -0.6\theta$, respectively. We observe that the order in which the linear chromophores are populated by the exciton depends on the polarization of the light pulse. That is, the direction of circular polarization of the light determines whether the exciton rotates clockwise or anticlockwise around the cycle. Evolution in the presence of a bath, as simulated via Redfield theory, is presented in the SI.

It is worth noting that the dependence of exciton rotational dynamics on pulse polarization is contingent upon the geometric arrangements of the linear chromophores relative to the axis of light propagation. In the model we present here, this angle is different for the two linear chromophores, *i.e.*, $\theta_a \neq \theta_b$. If, on the other hand, $\theta_a = \theta_b$, which would occur if the two linear chromophores were mutually parallel, then no local phase will be introduced

into the system and the effect of circularly polarized light on exciton rotation vanishes.

To quantify exciton rotation within the cyclic circuit, we calculate the normalized flux using Eq. 18 for the clockwise path: F_{23}, F_{31} and F_{12}. Furthermore, we define the total clockwise flux through site i as $F_i = F_{ji} - F_{ik}$, where j and k are the two sites neighboring site i. The calculated fluxes are plotted in Fig. S4. For the three-chromophore cycle the condition $F_{mn} = -F_{nm}$ holds for any given site, but the total flux coming in and out of the site is not necessarily equivalent. For example, for site 1 (*i.e.*, linear chromophore a), the net clockwise flux is given by $F_1 = F_{12} - F_{31} \neq 0$. However, because the construct is a closed ring and it is isolated from the environment, the sum of the net clockwise flux for all three sites must vanish by definition.

The direction of exciton flow is not easily inferred from the dynamics plotted in Figs. 4 and S3. To make studying flow easier, we define the total clockwise flux as $F_{\text{right}} = F_{23} + F_{31} + F_{12} = -F_{\text{left}}$. With this definition, $F_1 + F_2 + F_3 = F_{\text{right}} - F_{\text{left}} = 0$. We find that when an RCP pulse is used $F_{\text{right}} = 1.65 - 17.2i$ and an LCP pulse leads to $F_{\text{right}} = -2.04 - 17.3i$ eV. From this calculation, we clearly see that switching the polarization of light inverts the global direction of the exciton flow. Notably, $F_{\text{right}}^{(\text{RCP})} \neq F_{\text{left}}^{(\text{LCP})}$ due to differences in electronic coupling between the sites, arising from differences in the phases θ^a and θ^b.

To further explore the capability of CVCs to direct excitons around cyclic circuits, we constructed an expanded six-chromophore cyclic circuit. The results of this system study, presented in the SI, lead to similar conclusions. That is, exciting with right- or left-hand circularly polarized light induces flow in a clockwise or anticlockwise direction around the ring. From a practical standpoint, larger rings are more complicated, not just because they contain more molecules, but also because they require the alternation of real- and complex-valued coupling (via alternating linear and circular chromophores) in order to generate phase across the entire ring.

4.3 Branched excitonic circuit.

In addition to driving circular flow in ring-like circuits, complex-valued coupling can enable excitons to be directed along specific paths in branched circuits. To demonstrate this capability, we designed a model of branched circuits with two paths of linear chromophores originating from a central circular chromophore. This circuit is illustrated in Fig. 5A. A Hamiltonian describing this system is given by,

$$\hat{H}_{\text{spath}} = \begin{pmatrix} E_{\text{L}}^{a} & V_{\text{LL}} & 0 & 0 & 0 \\ V_{\text{LL}} & E_{\text{L}}^{a} & V_{\text{LC}}^{a} & 0 & 0 \\ 0 & V_{\text{CL}}^{a} & E_{\text{C}} & V_{\text{CL}}^{b} & 0 \\ 0 & 0 & V_{\text{LC}}^{b} & E_{\text{L}}^{b} & V_{\text{LL}} \\ 0 & 0 & 0 & V_{\text{LL}} & E_{\text{L}}^{b} \end{pmatrix}, \tag{20}$$

where the central circular chromophore has energy E_{C}, the two linear chromophores of the left branch both have energies E_{L}^{a} and the two linear chromophores of the right branch both have energies E_{L}^{b}. The topology of the circuit can be deduced based on the structure of the Hamiltonian matrix. As with the previous examples, the energies of the circular and

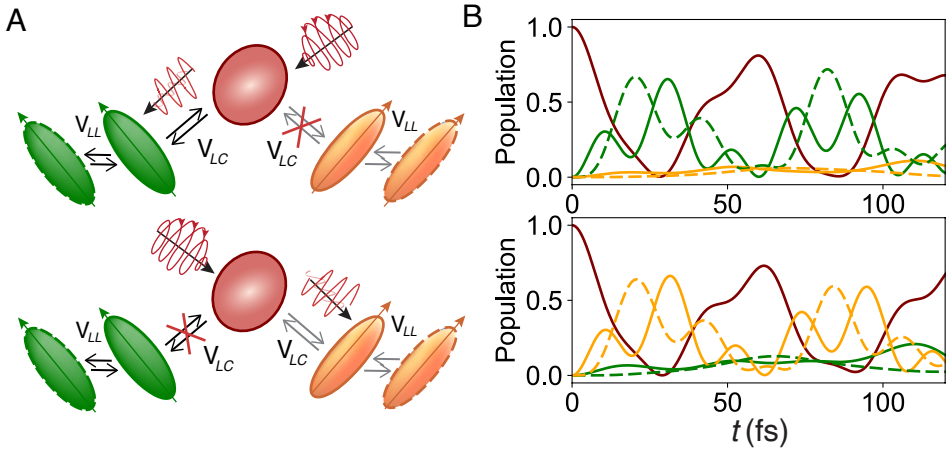

Figure 5: (A) System described by the Hamiltonian Eq. 20, consisting of two separate linear circuits connected to the same central $D_{N\text{h}}$ molecule. The cases when the phase is set to $\theta = 0$ and $\pi/2$ are illustrated, resulting in the green and orange paths being blocked, respectively. (B) The populations for both cases are calculated, evidencing that the population flux is almost completely stopped by careful manipulation of θ. The top and bottom plots correspond to the diagrams on the left.

linear molecules are taken as those for Mg-Porphyrin and Cy3, respectively, and all the linear chromophores have identical energies (*i.e.*, $E_{\mathrm{L}}^{a} = E_{\mathrm{L}}^{b} = E_{Cy3}$ and $E_{\mathrm{C}} = E_{MgPh}$. The coupling between the circular and linearly excited sites is defined with Eq. 9, and the phase θ is different for each branch (*i.e.*, $\theta_{\mathrm{L}}^{a} = \theta_{\mathrm{L}}^{b}$ and $\theta_{R}^{a} = \theta_{R}^{b}$). For simplicity, the linear-to-linear coupling V_{LL} is set to half the energy difference ΔE_{LC}.

Starting from an exciton fully localized on the central molecule via a circularly-polarized pulse (red circle in Fig. 5A), the amount of population flowing into each of the two connected molecules depends on their relative angle with respect to the incident light. When the connected chromophores (green and orange solid lines) are placed orthogonally with respect to each other (for example, by setting $V_{x}^{a} = V_{y}^{b}$), the exciton flux is completely blocked when the incident light is directed parallel to one set of molecules (no flux), and orthogonal to the other (full flux). In the example shown in Fig. 5A, when the light is parallel to the green path and orthogonal to the orange one, the first path is blocked (top diagram). When the light is parallel to the orange chromophores, this path is blocked instead (bottom diagram). Note that a full delocalization across the circular and all the linear chromophores in the activated path (both solid and dashed lines) can be achieved by aligning the linear molecules parallel to each other.

We calculated the exciton populations for this model, setting $V_{\mathrm{LC,a}}^{x} = V_{\mathrm{LC,b}}^{y} = 5\Delta\epsilon_{\mathrm{LC}}/4$ and $V_{LC,a}^{y} = V_{LC,b}^{x} = \Delta\epsilon_{\mathrm{LC}}/4$. We find that switching the relative phase, $\theta = \theta_{a} = \theta_{b}$, between 0 and $\pi/2$ almost completely blocks the flux to the orange and green paths, respectively. This concept can be generalized for complex constructs connecting more than two paths with similar results.

We note that in this particular circuit architecture, the direction of the circularly polarized light has no effect on the direction of exciton flux. The direction of exciton flux in the branched circuit is determined by the angles of the linear chromophores relative to the direction of light propagation. Therefore, switching between RCP and LCP light will not change the exciton flux in Fig. 5. This is analogous to observations that the AB effect does

not manifest in open cycles.[25] In fact, one can argue that circularly polarized light is not strictly necessary in this particular construct. A similar phase control could be achieved with a linear pulse on a circuit of chromophore molecules with precisely aligned dipole moment vectors. Indeed, the control of the phase is an artifact of the alignment between the molecules and does not necessarily arise for the complex phase in the coupling. We discuss this issue further in the SI.

4.4 Analysis of implementation error

The dynamics of delocalized excitons in the cyclic and branched circuits are influenced by their alignment relative to incident light, as characterized by angle θ. Achieving precise alignment in an experimental setting is challenging, resulting in variations from the intended angle by $\delta\theta$. At the same time, unless we have access to precise single-molecule measurement frameworks, observed signatures will typically reflect an ensemble of circuits, with an associated distribution of $\delta\theta$ angles. These variations will be influenced by factors such as laser alignment precision or the synthetic accuracy of chromophore positioning.

For the 3-chromophore circuit, implementation errors could hinder the intended exciton flow reversal with changing light direction. This manifests as a bias in exciton delocalization toward a linear chromophore optimally oriented to the light pulse, regardless of the light's circular polarization used. Such an error is quantifiable by comparing the populations of the two linear chromphores under a different light direction (*e.g.,* RCP or LCP light), with no discrepancy indicating perfect flow reversal:

$$\varepsilon_{\text{trimer}}(\delta\theta) = \langle |P_a^{\text{RCP}}(\delta\theta) - P_b^{\text{LCP}}(\delta\theta)| \rangle_t. \tag{21}$$

Here, $\varepsilon_{\text{trimer}}$ represents the time-averaged difference in chromophore populations $P_i = \hat{\rho}_{ii}(t)$ under right (RCP) and left (LCP) circularly polarized light. The vector $\delta\theta$ encompasses the range of angle deviations for each molecular orientation and light polarization.

In the branched circuit, misalignment can cause erroneous exciton populations in the non-targeted branch. This error is similarly evaluated as a time-weighted average:

$$\varepsilon_{\text{branch}}(\delta\theta) = \langle |P_i^1(\delta\theta) + P_i^2(\delta\theta)| \rangle_t. \tag{22}$$

Here, $P_i^{1,2}$ denotes the populations of the molecules on the unselected branch. According to the notation introduced in the Hamiltonian $\hat{H}_{\text{spath}}$, for instance, $P_i^1 = \hat{\rho}11(t)$ and $P_i^2 = \hat{\rho}_{33}(t)$ when the intended branch is b, while $P_i^1 = \hat{\rho}_{22}(t)$ and $P_i^2 = \hat{\rho}_{44}(t)$ apply when branch a is the target.

We assess the implementation error for both circuits by simulating an ensemble of 500 configurations with $\delta\theta$ varying within $[-\pi/12, \pi/12]$. For the three-chromophore circuit, the error is estimated to be around 0.132, assuming random deviations for each chromophore and polarization direction. Remarkably, switching between right and left light polarization at a constant $\delta\theta$ deviation leads to an error of nearly zero for the three-chromophore cyclic circuit, $\varepsilon_{\text{trimer}}$. This approximation is not unreasonable for a precise experimental setup, where switching light polarization does not usually imply a modification in the orientation of the light with respect to the pulse.

The branched circuit yields an implementation error of approximately 0.176 under random deviations, $\delta\theta$, from angles set to those in Fig. 5. This error is not significantly higher than the error at $\delta\theta = 0$ (approximately 0.113), suggesting that random alignment errors minimally affect ensemble measurements.

It is worth noting that misalignment of the circular chromophore with the light pulse's xy-plane, represented by angle ϕ, primarily introduces a global phase shift without significantly affecting population outcomes (see Eq. 15).

5 Conclusions

In this manuscript, we have described a method to introduce a complex phase into the electronic coupling between interacting chromophores. We have demonstrated that RCP and LCP light can be used to control the sign of this phase, while its magnitude can be manipulated by changing the angle of the incident light with respect to the linear chromophore, either through modifying the laser parameters or the geometrical orientation of the molecules. The effect presented here could have important implications for the development of efficient organic semiconductor materials, providing a strategy for directional excitonic flux in the coherent electron transfer regime. To provide a simple and tractable model for the imaginary coupling we assumed the environment only couples weakly to the system. Still, we anticipate our model can be easily expanded to include the effect of strong system-bath interactions.

We also commented on the challenges associated with the physical implementation of a system with CVCs. These challenges, can be divided into those associated with 1) implementation and 2) measurement of the resulting populations. We found errors in both implementation and measurement to arise from deviations in the alignment of the *linear* components of the circuit with respect to the pulse. Although errors in the implementation can lead to significant errors in the populations of a single system when the deviation is large, measurement of large ensembles leads to reduced average deviations. For the three-chromophore cycle, the measurement error is negligible, and for the branched-circuit the error is relatively small as well. The alignment of the *circular* molecule with respect to the plane of light was, on the other hand, observed to contribute only a global phase to the exciton evolution. Therefore, our results demonstrate promising avenues for the implementation of geometrical phase control via complex-valued intermolecular couplings.

Acknowledgement

This work was supported by the US Department of Energy (DOE), Office of Science, Basic

Energy Sciences (BES) under award DE-SC0019998. M.A.C acknowledges financial support from the Molecular Sciences Software Institute (MolSSI) Software Fellowship program. M.A.C thanks Prof. Jianshu Cao, Amro Dodin and Ardavan Farahvash for helpful discussions.

Supporting Information Available

Derivation of the time-dependent wavefunction coefficients for the *linear-circular* dimer system and the equations of motion for the closed and open system with the Redfield model. The populations for the dimer and three-chromophore cycle simulated on an open system. The calculated flux for the three-chromophore cycle with RCP and LCP pulses, and population dynamics for a six-chromophore ring and the branched circuit using a linear pulse.

References

(1) Förster, T. Intermolecular Energy Migration and Fluorescence. *Annals of Physics (Leipzig)* **1948**, *2*, 55–75.

(2) Scholes, G. D.; Jordanides, X. J.; Fleming, G. R. Adapting the Förster theory of energy transfer for modeling dynamics in aggregated molecular assemblies. *The journal of physical chemistry B* **2001**, *105*, 1640–1651.

(3) Mikhnenko, O. V.; Blom, P. W.; Nguyen, T. Q. Exciton diffusion in organic semiconductors. *Energy and Environmental Science* **2015**, *8*, 1867–1888.

(4) Ostroverkhova, O. Organic Optoelectronic Materials: Mechanisms and Applications. **2016**, *116*, 13279–13412.

(5) Scholes, G. D.; Fleming, G. R.; Olaya-Castro, A.; Van Grondelle, R. Lessons from nature about solar light harvesting. *Nature Chemistry* **2011**, *3*, 763–774.

(6) Brédas, J. L.; Sargent, E. H.; Scholes, G. D. Photovoltaic concepts inspired by coherence effects in photosynthetic systems. *Nature Materials 2017 16:1* **2016**, *16*, 35–44.

(7) Wang, H.; Jiang, S.; Chen, S.; Zhang, X.; Shao, W.; Sun, X.; Zhao, Z.; Zhang, Q.; Luo, Y.; Xie, Y. Insights into the excitonic processes in polymeric photocatalysts. *Chem. Sci.* **2017**, *8*, 4087–4092.

(8) Jares-Erijman, E. A.; Jovin, T. M. FRET imaging. *Nature Biotechnology 2003 21:11* **2003**, *21*, 1387–1395.

(9) Jares-Erijman, E. A.; Jovin, T. M. Imaging molecular interactions in living cells by FRET microscopy. *Current opinion in chemical biology* **2006**, *10*, 409–416.

(10) Butov, L. V. Excitonic devices. *Superlattices and Microstructures* **2017**, *108*, 2–26.

(11) So, F.; Kido, J.; Burrows, P. Organic light-emitting devices for solid-state lighting. *MRS bulletin* **2008**, *33*, 663–669.

(12) Pope, M.; Kallmann, H. P.; Magnante, P. Electroluminescence in organic crystals. *The Journal of Chemical Physics* **1963**, *38*, 2042–2043.

(13) Castellanos, M. A.; Dodin, A.; Willard, A. P. On the design of molecular excitonic circuits for quantum computing: The universal quantum gates. *Phys.Chem. Chem. Phys.* **2020**, *22*, 3048–3057.

(14) Castellanos, M. A.; Willard, A. P. Designing excitonic circuits for the Deutsch-Jozsa algorithm: mitigating fidelity loss by merging gate operations. *Physical Chemistry Chemical Physics* **2021**, *23*, 15196–15208.

(15) Chenu, A.; Scholes, G. D. Coherence in energy transfer and photosynthesis. *Annual Review of Physical Chemistry* **2015**, *66*, 69–96.

(16) Scholes, G. D.; Rumbles, G. Excitons in nanoscale systems. *Nature materials* **2006**, *5*, 683–696.

(17) Labastide, J. A.; Thompson, H. B.; Marques, S. R.; Colella, N. S.; Briseno, A. L.; Barnes, M. D. Directional charge separation in isolated organic semiconductor crystalline nanowires. *Nature Communications* **2016**, *7*, 1–7.

(18) Cohen-Tannoudji, C.; Diu, B.; Laloë, F. *Quantum Mechanics*; John Wiley & Sons, 1977; Vol. 1.

(19) Aharonov, Y.; Bohm, D. Significance of electromagnetic potentials in the quantum theory. *Physical Review* **1959**, *115*, 485–491.

(20) Simmons, S.; Wu, H.; Morton, J. J. Controlling and exploiting phases in multi-spin systems using electron spin resonance and nuclear magnetic resonance. *Philosophical Transactions of the Royal Society A: Mathematical, Physical and Engineering Sciences* **2012**, *370*, 4794–4809.

(21) Monroe, C.; Campbell, W. C.; Duan, L.-M.; Gong, Z.-X.; Gorshkov, A. V.; Hess, P. W.; Islam, R.; Kim, K.; Linke, N. M.; Pagano, G.; Richerme, P.; Senko, C.; Yao, N. Y. Programmable quantum simulations of spin systems with trapped ions. *Rev. Mod. Phys.* **2021**, *93*, 025001.

(22) Borunda, M. F.; Liu, X.; Kovalev, A. A.; Liu, X. J.; Jungwirth, T.; Sinova, J. Aharonov-Casher and spin Hall effects in mesoscopic ring structures with strong spin-orbit interaction. *Physical Review B - Condensed Matter and Materials Physics* **2008**, *78*, 245315.

(23) Grbić, B.; Leturcq, R.; Ihn, T.; Ensslin, K.; Reuter, D.; Wieck, A. D. Aharonov–Bohm oscillations in p-type GaAs quantum rings. *Physica E: Low-dimensional Systems and Nanostructures* **2008**, *40*, 1273–1275.

(24) Cao, J.; Silbey, R. J. Optimization of exciton trapping in energy transfer processes. *Journal of Physical Chemistry A* **2009**, *113*, 13825–13838.

(25) Engelhardt, G.; Cao, J. Tuning the Aharonov-Bohm effect with dephasing in nonequilibrium transport. *Physical Review B* **2019**, *99*, 1–12.

(26) Yuen-Zhou, J.; Saikin, S. K.; Yao, N. Y.; Aspuru-Guzik, A. Topologically protected excitons in porphyrin thin films. *Nature Materials* **2014**, *13*, 1026–1032.

(27) Hestand, N. J.; Spano, F. C. Molecular aggregate photophysics beyond the Kasha model: Novel design principles for organic materials. *Accounts of chemical research* **2017**, *50*, 341–350.

(28) Gorman, J.; Hart, S. M.; John, T.; Castellanos, M. A.; Harris, D.; Parsons, M. F.; Banal, J. L.; Willard, A. P.; Schlau-Cohen, G. S.; Bathe, M. Sculpting photoproducts with DNA origami. *Chem* **2024**,

(29) Davydov, A. S. THE THEORY OF MOLECULAR EXCITONS. *Soviet Physics Uspekhi* **1964**, *7*, 145–178.

(30) Frenkel, J. On the transformation of light into heat in solids. I. *Physical Review* **1931**, *37*, 17.

(31) Hestand, N. J.; Spano, F. C. Expanded theory of H-and J-molecular aggregates: the effects of vibronic coupling and intermolecular charge transfer. *Chemical reviews* **2018**, *118*, 7069–7163.

(32) Hart, S. M.; Banal, J. L.; Castellanos, M. A.; Markova, L.; Vyborna, Y.; Gorman, J.; Häner, R.; Willard, A. P.; Bathe, M.; Schlau-Cohen, G. S. Activating charge-transfer state formation in strongly-coupled dimers using DNA scaffolds. *Chemical science* **2022**, *13*, 13020–13031.

(33) Shi, L.; Willard, A. P. Modeling the effects of molecular disorder on the properties of Frenkel excitons in organic molecular semiconductors. *Journal of Chemical Physics* **2018**, *149*, 94110.

(34) Barth, I.; Manz, J.; Shigeta, Y.; Yagi, K. Unidirectional electronic ring current driven by a few cycle circularly polarized laser pulse: Quantum model simulations for Mg-porphyrin. *Journal of the American Chemical Society* **2006**, *128*, 7043–7049.

(35) Barth, I.; Manz, J. Electric ring currents in atomic orbitals and magnetic fields induced by short intense circularly polarized π laser pulses. *Physical Review A - Atomic, Molecular, and Optical Physics* **2007**, *75*.

(36) Laser-polarization effects on coherent vibronic excitation of molecules with quasi-degenerate electronic states. *Journal of Physical Chemistry A* **2012**, *116*, 11260–11272.

(37) Yang, P. Y.; Cao, J. Steady-State Analysis of Light-Harvesting Energy Transfer Driven by Incoherent Light: From Dimers to Networks. *Journal of Physical Chemistry Letters* **2020**, *11*, 7204–7211.

(38) Breuer, H. P.; Petruccione, F. *The Theory of Open Quantum Systems*; Oxford University Press, 2007; Vol. 1; pp 1–656.

TOC Graphic